

An application of a Si/CdTe Compton camera for the polarization measurement of hard x-rays from highly charged heavy ions

Yutaka Tsuzuki,^{1,2,a)} Shin Watanabe,^{3,2} Shimpei Oishi,⁴ Nobuyuki Nakamura,⁴ Naoki Numadate,^{4,5} Hirokazu Odaka,^{1,2} Yuusuke Uchida,⁶ Hiroki Yoneda,⁷ and Tadayuki Takahashi^{2,1}

¹⁾Department of Physics, The University of Tokyo, 7-3-1, Hongo, Bunkyo, Tokyo 113-0033, Japan

²⁾Kavli Institute for the Physics and Mathematics of the Universe (WPI), Institutes for Advanced Study (UTIAS), The University of Tokyo, 5-1-5 Kashiwa-no-Ha, Kashiwa, Chiba, 277-8583, Japan

³⁾Institute of Space and Astronautical Science, Japan Aerospace Exploration Agency, 3-1-1 Yoshinodai, Chuo Sagami-hara, Kanagawa, 252-5210, Japan

⁴⁾Institute for Laser Science, The University of Electro-Communications, Chofu, Tokyo 182-8585, Japan

⁵⁾Komaba Institute for Science, The University of Tokyo, 3-8-1 Komaba, Meguro, Tokyo 153-8902, Japan

⁶⁾Department of Physics, Hiroshima University, 1-3-1 Kagamiyama, Higashi-Hiroshima, Hiroshima 739-8526, Japan

⁷⁾RIKEN Nishina Center, 2-1 Hirosawa, Wako, Saitama 351-0198, Japan

(Dated: 10 March 2022)

The methods to measure the polarization of the x-rays from highly charged heavy ions with a significantly higher accuracy than the existing technology is needed to explore relativistic and quantum electrodynamics (QED) effects including the Breit interaction. We developed the Electron Beam Ion Trap Compton Camera (EBIT-CC), a new Compton polarimeter with pixelated multi-layer silicon and cadmium telluride counters. The EBIT-CC detects the three-dimensional position of Compton scattering and photoelectric absorption, and thus the degree of polarization of incoming x-rays can be evaluated. We attached the EBIT-CC on the Tokyo Electron Beam Ion Trap (Tokyo-EBIT) in the University of Electro-Communications. An experiment was performed to evaluate its polarimetric capability through an observation of radiative recombination x-rays emitted from highly charged krypton ions, which were generated by the Tokyo-EBIT. The Compton camera of the EBIT-CC was calibrated for the ~ 75 keV x-rays. We developed event reconstruction and selection procedures and applied them to every registered event. As a result, we successfully obtained the polarization degree with an absolute uncertainty of 0.02. This uncertainty is small enough to probe the difference between the zero-frequency approximation and full-frequency-dependent calculation for the Breit interaction, which is expected for dielectronic recombination x-rays of highly charged heavy ions.

I. INTRODUCTION

Polarization of hard x-rays emitted through interactions between highly charged heavy ions and electrons is of significant importance for diagnostics of relativistic quantum effects¹² as well as of non-thermal components in hot plasma⁵. An electron beam ion trap (EBIT) is a powerful device for studying such polarized x-rays, with which one can observe x-rays emitted from trapped highly charged ions interacting with a unidirectional mono-energy electron beam.

Polarization measurements with an EBIT have been performed using mainly two kinds of polarimeters so far. One of them is Bragg crystal polarimeters¹⁹. They are useful for x-rays with energies $\lesssim 10$ keV and thus are used for measuring the polarization of K x-rays from ions with an atomic number $Z \lesssim 30$ or L x-rays from med- Z (~ 50) ions. For example, Beiersdorfer et al.³ measured the polarization of x-rays with energies $\simeq 6.7$ keV from helium-like iron (Fe) using a crystal polarimeter. The

other is Compton polarimeters which employ light materials such as beryllium (Be). Their typical energy range is 10 – 30 keV and hence they are suitable for measuring the polarization of K x-rays emitted through dielectronic recombination (DR) from highly charged krypton (Kr) and xenon (Xe). For example, Shah et al.¹⁸ measured the degree of polarization of DR x-rays emitted from highly charged Kr ions, using a Compton polarimeter with a Be scatterer and an absorber with Si-PIN diodes.

By contrast, for K x-rays of heavier ions with $Z \gtrsim 80$, where strong relativistic and quantum electrodynamics (QED) effects are expected, a polarimeter sensitive for a higher energy range, such as 70 - 80 keV, is needed. Furthermore, higher sensitivity and polarimetric capability than the existing polarimeters are also necessary to explore the nature of the relativistic and QED effects, such as the limitation of the zero-frequency approximation in the Breit interaction^{4,10,12,14}. The Breit interaction is often calculated by assuming the frequency of the virtual photon that is exchanged between the interacting electrons to be zero. This zero-frequency approximation generally yields sufficient accuracy, *i.e.*, the difference between the approximation and full-frequency-dependent calculation is small in most cases. Tong et al.²³ calculated

^{a)}Electronic mail: yutaka.tsuzuki@ipmu.jp

the polarization of x-rays emitted in dielectronic recombination of lithium-like ions and showed that the approximation modifies the degree of polarization by ~ 0.02 for heavy elements with $Z \sim 80$. It is still difficult to probe the difference between the zero-frequency approximation and full-frequency-dependent calculation with any of the methods stated above.

Recently, novel Compton cameras that employ silicon (Si) and cadmium telluride (CdTe) semiconductor detectors have been developed as promising polarimeters for x-ray and gamma-ray observations in field of astrophysics^{21,25}. Indeed, a Si/CdTe Compton camera, developed for observations of high-energy celestial objects, was adopted as the Soft Gamma-ray Detector (SGD) onboard the *Hitomi* satellite²⁶. *Hitomi* has succeeded in detecting the polarized hard x-ray emission from the Crab nebula⁷.

Katsuta et al.⁸ studied the polarimetric capability of a Si/CdTe Compton camera with experiments using a synchrotron beam facility, SPring-8, and demonstrated that the Si/CdTe Compton camera had excellent polarimetric performance of detecting the degree of polarization with a $\lesssim 3\%$ uncertainty, proving its great potential.

We have developed a new Si/CdTe Compton camera containing pixelated multi-layer semiconductor detectors. It is capable of determining the three-dimensional position of interactions between incoming photons and detector materials inside each layer, and therefore the degree of polarization of the photons can be determined with it more precisely than any other methods to date. In addition, large thickness of the stacked layers (~ 2 cm for the Si layers) results in high efficiency ($\sim 50\%$ at around 70 keV) for detecting photons.

Our question is whether the polarimetry of hard x-rays emitted from highly charged ions advances by applying the Compton camera. Here we demonstrate the polarimetric performance of our Si/CdTe Compton camera by measuring radiative recombination x-rays emitted from highly charged Kr ions that are generated by an EBIT.

In this paper we present the principles and methods of the polarimetry with our Compton camera and the results of the experiment. In Section II, we outline the principles and specifications of the Compton camera. In Section III, the experimental setup and conditions are explained. In Section IV, we describe the method of the calibration, Monte Carlo simulation, and data analysis. Section V gives the result of the experiment and discussions on the systematic uncertainties of our result. Summary and conclusion are presented in Section VI.

II. COMPTON CAMERA

A. Principle

Compton cameras utilize Compton scattering to obtain information of energy and direction of incoming photons. One can also evaluate the degree of polarization by an-

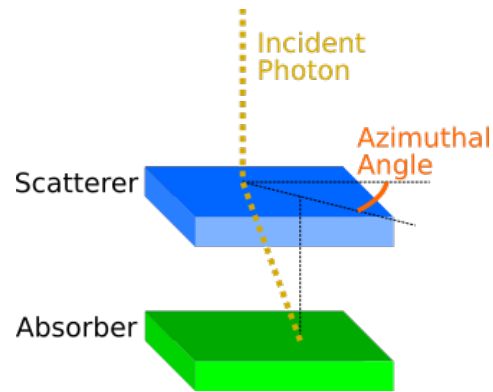


FIG. 1. A schematic drawing of polarization measurement with a Compton camera.

alyzing the scattering angles of photons. In general, a Compton camera consists of at least one scatterer and one absorber (see Fig. 1). In a Compton camera, incident x-ray photons can be scattered by the scatterer and then are photo-absorbed by the absorber¹⁵.

Since the differential cross section for Compton scattering depends on the polarization angle and is modulated by a squared cosinusoidal term, the degree of polarization of an incident photon beam is measurable with Compton cameras by counting the events where photons are scattered by the scatterer and are absorbed by the absorber. The differential cross section for Compton scattering off a free electron at rest is given by the following Klein-Nishina formula⁹:

$$\frac{d\sigma}{d\Omega} = \frac{r_0^2}{2} \left(\frac{E}{E_0} \right)^2 \left(\frac{E}{E_0} + \frac{E_0}{E} - 2 \sin^2 \theta \cos^2(\phi - \phi_0) \right), \quad (1)$$

where $r_0 = 2.818 \times 10^{-15}$ m is the classical electron radius, E_0 is the initial energy of the incident photon, E is the energy of the scattered photon, θ is the scattering polar angle, ϕ is the azimuthal scattering angle, and ϕ_0 is the polarization angle of the photon. In reality, electrons are bound to atoms and are not at rest, and thus the distribution of the scattered photons is affected by the so-called Doppler broadening^{17,27}.

The degree of polarization of incoming x-rays can be calculated by comparing the two distributions of ϕ , namely the measured and simulated ones. We usually employ Monte Carlo simulations to obtain the azimuthal distribution model of the events $d^{(\text{model})}(\phi)$ and fit the experimental distribution $d^{(\text{exp})}(\phi)$ with it (see Sec. V for detail). By dividing $d^{(\text{exp})}(\phi)$ by the simulated distribution for an unpolarized beam $d^{(0)}(\phi)$, we obtain a modulation curve that contains a component proportional to $\cos(2\phi - \text{const.})$.

B. The Electron Beam Ion Trap Compton camera (EBIT-CC)

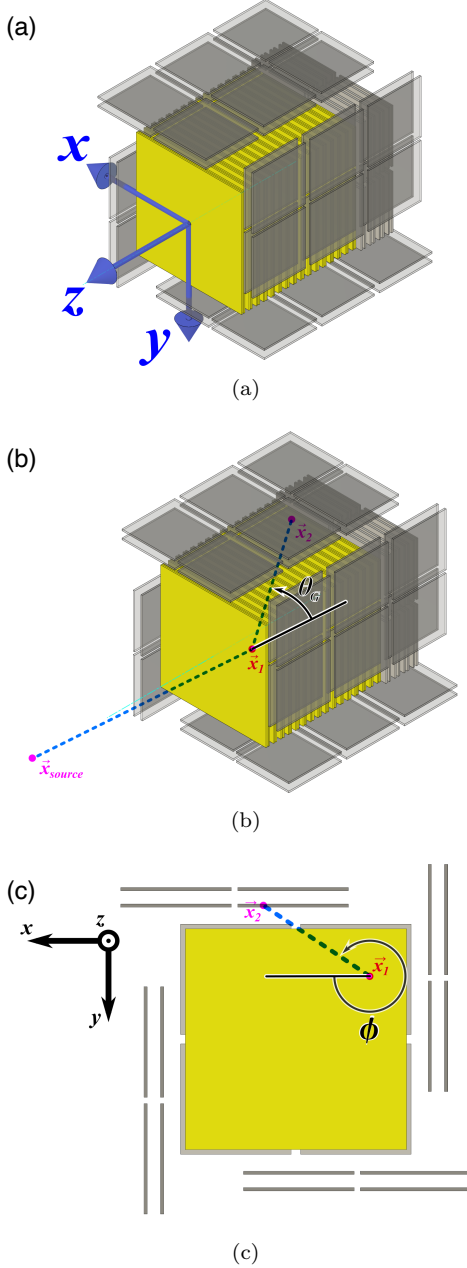


FIG. 2. Schematics and coordinates definition of the detector parts of the EBIT-CC. Yellow and gray parts show the Si and the CdTe detectors, respectively. (a) A schematic of the coordinate system of the EBIT-CC. Its origin is located at the center on the first layer of the Si detectors. (b) Definition of the geometrical scattering angle θ_G . Blue dotted line depicts an incoming x-ray from the source \vec{x}_{source} , which is scattered at \vec{x}_1 and absorbed at \vec{x}_2 . (c) Definition of the azimuthal angle ϕ .

We developed a new type of Si/CdTe Compton camera system for experiments with an EBIT, named the Elec-

tron Beam Ion Trap Compton camera (EBIT-CC). It has the same structure as that of the Compton camera of the *Hitomi* SGD. We used a new set of parameters of electric devices so that the EBIT-CC covers lower energy range compared to the SGD. The dimensions of the EBIT-CC are roughly $12 \text{ cm} \times 12 \text{ cm} \times 12 \text{ cm}$.

The Compton camera in the EBIT-CC employs Si detectors mainly as scatterers and CdTe detectors as absorbers. The Compton camera contains three parts of detector clusters, namely Si detector part, CdTe bottom detector part, and CdTe side detector part (see Fig. 2). Si detector part has 32 layers of Si detectors, each of which is pixelated into 16×16 pixels to enable it to detect the interaction position of photons. The thickness of a single Si layer is $600 \mu\text{m}$, and accordingly the total thickness amounts to 1.92 cm , by which we obtain sufficiently high Compton scattering probability ($\sim 50\%$ at 75 keV). CdTe bottom and side detector parts are respectively composed of 8 layers and 4×2 layers of CdTe detectors. The CdTe detectors are arranged to surround the Si detector part. A CdTe bottom layer is pixelated into 16×16 pixels, whereas a CdTe side layer is pixelated into 16×24 pixels. The thickness of a CdTe layer is $750 \mu\text{m}$. The size of each pixel is $3.2 \text{ mm} \times 3.2 \text{ mm}$ both for the Si and the CdTe layers. Their design details are shown in Watanabe et al.²⁶ and Tajima et al.²⁰

The charge signals generated in the detector material are amplified and converted to digital signals by 64-channel application-specific integrated circuits (ASICs). One ASIC has 8×8 channels, and hence a Si, CdTe bottom, and CdTe side layers are connected to 4, 4, and 6 ASICs, respectively. The total numbers of ASICs and channels are 208 and 13312, respectively.

III. EXPERIMENT

We performed an experiment to measure the degree of linear polarization of the 75 keV x-rays that are emitted through the radiative recombination to $n = 1$ state from fully-ionized and hydrogen-like Kr ions. We explain the detail in this section.

We constructed the experiment apparatus by combining the EBIT-CC and a germanium (Ge) detector with the Tokyo Electron Beam Ion Trap (Tokyo-EBIT)^{13,24} at the University of Electro-Communications (UEC). A schematic view of the setup is shown in Fig. 3. Here, the EBIT-CC and the Ge detector are for polarimetry and for spectroscopy, respectively.

The Tokyo-EBIT generates fully-ionized and hydrogen-like Kr ions. It is composed of an electron gun and an ion drift tube. The electron beam travels along the y axis of the Compton camera (see Fig. 2) toward the $-y$ direction and ionizes Kr with electron collision. Highly charged ions generated by the beam are confined in the ion trap. The electron beam energy and current were 58.0 keV and 130 mA , respectively. The typical electron beam radius is $30 \mu\text{m}$ ⁶

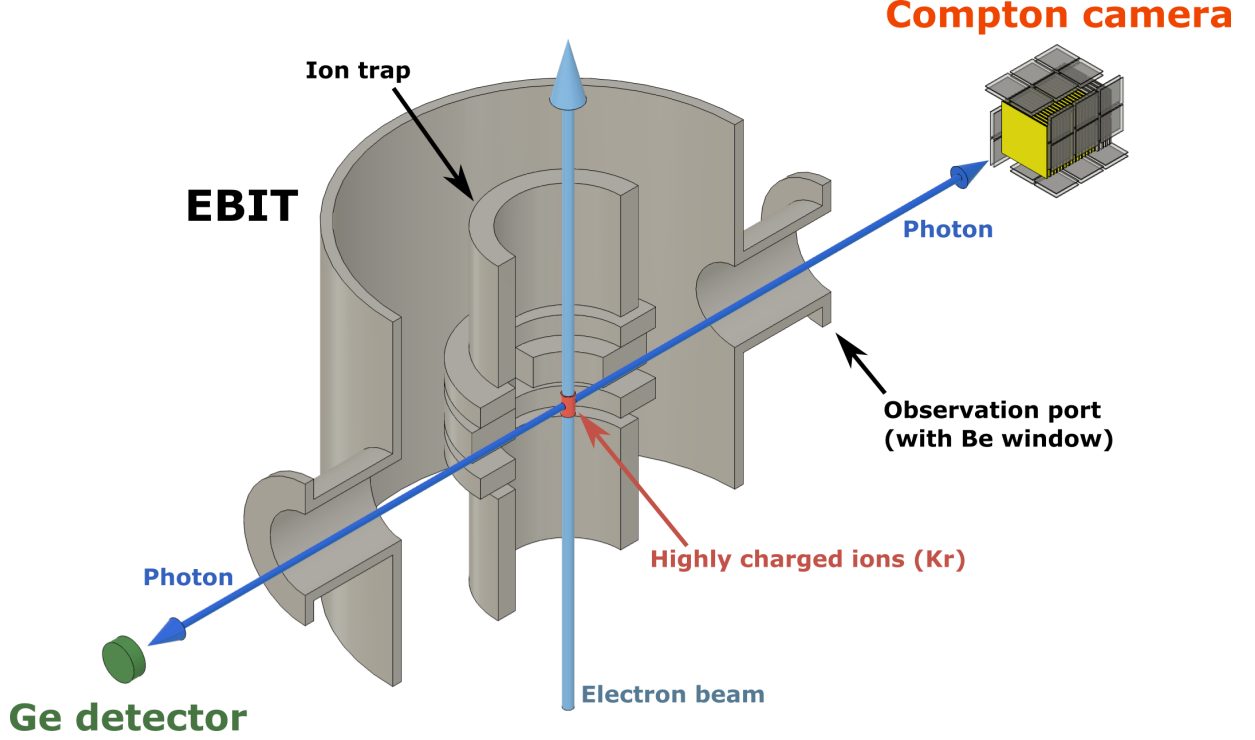


FIG. 3. Schematic view of our experiment setup. The ion trap in the EBIT captures highly charged Kr ions, which are ionized by the electron beam. Radiative recombination x-rays emitted from the ions are transmitted to the Compton camera or to the Ge detector through the observation ports with Be windows. We employ the Ge detector and the EBIT-CC as a spectrometer and a polarimeter, respectively.

and the height (length in the y direction) of the radiating area was evaluated to be smaller than 10 mm. The strength of the magnetic field in the trap region was 4 T. Kr gas was injected into the Tokyo-EBIT through a gas injector. The Kr ions were stored with an axial trapping potential of 100 V and dumped every 30 s to avoid the accumulation of contaminant heavy ions. The x-rays generated in the EBIT were radiated to detectors through Be windows, whose effective diameters are 50 mm for the EBIT-CC and 25 mm for the Ge detector.

The Compton camera was placed approximately 500 mm away from the center of the EBIT. The operational temperature of the Compton camera was kept low at -20°C to suppress the leakage current of the detectors. The bias voltages were set to 230 V and 1000 V for the Si and CdTe detectors, respectively. To reduce noise, the energy threshold of the Si detectors was set to approximately 8 keV, which corresponds to the scattering angle $\theta_K \gtrsim 80^\circ$ where the total energy is 75 keV (see Section IV for the definition of θ_K). Then, most of the Compton scattered photons should be absorbed in the Si or CdTe-side part. The trigger for the CdTe-bottom part was disabled. The calibration procedure and the

energy resolution of the Compton camera are described and discussed in Section IV.

The Ge detector was ORTEC GLP-36360/13 and was placed at the opposite side of the Compton camera with respect to the EBIT. The energy resolution of the Ge detector was 595 eV (0.73 %) in full width at half maximum (FWHM) at 81 keV. The diameter and depth of its sensitive volume are 36 mm and 13 mm, respectively.

IV. CALIBRATION, SIMULATION, AND DATA ANALYSIS

In this section, we outline the method for data analysis. A raw event obtained with the EBIT-CC is composed of an array of ADC charge values q_i and of pixel IDs ID_i . From each set of hits $\{(q_i, ID_i); i = 1, 2, \dots, N_{\text{hit}}\}$ the event data is processed in the following steps.

First, q_i are converted to the corresponding energy values E_i by using calibration functions and ID_i are converted to their positions \vec{x}_i . We obtain the set $\{(E_i, \vec{x}_i); i = 1, 2, \dots, N_{\text{hit}}\}$.

The second step is the event reconstruction, that is,

mainly to determine the most probable sequence of the hits. We obtain the kinematic θ_K , geometrical θ_G and the azimuthal scattering angle ϕ , for each set. Here, θ_K is defined from the kinematics of Compton scattering as:

$$\cos \theta_K = 1 - m_e c^2 \left(\frac{1}{E - E_S} - \frac{1}{E} \right) \quad (2)$$

where E and E_S denote the total photon energy and its energy deposit on the scatterer, respectively. The other parameter θ_G is defined as the angle between the momenta of the incoming photon and of the scattered photon (see Fig. 2).

The third step is event selection. We impose several conditions on total energy, θ_K , θ_G , and hit sequence. Details are described in Subsection IV C.

A. Event reconstruction

The event reconstruction, that is, to determine the ordering of hits $\{(E_i, \vec{x}_i); i = 1, 2, \dots, N_{\text{hit}}\}$, is necessary to calculate θ_K , θ_G , and ϕ . In this subsection we formulate a simple method of the reconstruction.

For the events of the total energy E in a range of $73.0 \text{ keV} < E < 77.5 \text{ keV}$, 94.0% of the registered events containing Compton scattering are found to be two-hit events. Thus, we consider here only the two-hit Compton-scattered events and describe each of these events as $\{(E_1, \vec{x}_1), (E_2, \vec{x}_2)\}$. With an aid of the Compton kinematics and the relation $2E \simeq 2 \times 75 \text{ keV} < m_e c^2 = 511 \text{ keV}$, the energy deposit on the scatterer E_S is straightforwardly deduced to be smaller than that on the absorber E_A , as given by,

$$\begin{aligned} E_A - E_S &= 2E_A - E \\ &= E \left(\frac{2}{1 + \frac{E}{m_e c^2} (1 - \cos \theta)} - 1 \right) \\ &\geq E \left(\frac{2}{1 + 2E/m_e c^2} - 1 \right) > 0. \end{aligned} \quad (3)$$

Therefore $E_S = \min\{E_1, E_2\}$ and $E_A = \max\{E_1, E_2\}$. The sequence of the two hits is also determined with this set of equations.

Once the event has been reconstructed, θ_K is calculated as in Eq. 2. In addition, θ_G and ϕ are computed as in Fig. 2. The position of the trapped ions, \vec{x}_{source} , which is necessary to compute θ_G , is obtained with a Compton imaging technique²². Here, we define two types of sequence: (1) *Si-Si sequence* where a photon is scattered in a Si detector and absorbed in another Si detector, and (2) *Si-CdTe-side sequence* where a photon is scattered in a Si detector and absorbed in a CdTe-side detector.

B. Calibration

To perform the event selection appropriately, precise energy calibration of the Compton camera is of particu-

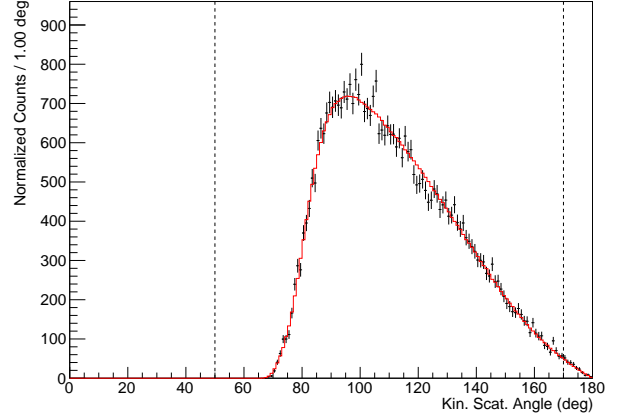


FIG. 4. Distributions of θ_K of the events that satisfy all the selection criteria except for (3) (see text). Data points (black) show the Kr measurement minus the background. Solid line (red) shows the simulation. Dotted lines show criterion (3).

lar importance. In this experiment, we optimized the settings of the ASICs for x-rays with the energy $\sim 75 \text{ keV}$, which is lower than those adopted for the *Hitomi* SGD.

The procedure of calibrating the Compton camera consists of three steps. First, the non-uniformity of the outputs from the ADCs for each channel within an ASIC was evaluated by inputting constant charge pulses called *test pulse* into each channel. Then the outputs from the ADCs within an ASIC could be treated in the same manner regardless of the channel. Second, the conversion factors from the ADC value to energy were calculated using point sources of radio isotopes. Third, the energy outputs lower than the trigger threshold were corrected for each ASIC connected to a Si detector.

We performed the calibration, using gamma-rays from a ^{133}Ba source, and found the energy resolution of the Compton camera for reconstructed Compton events to be 4.7 keV (5.8%) in FWHM at $E_S + E_A \simeq 81 \text{ keV}$ after the event selection (see Subsection IV C). Note that this value was calculated by combining the outputs from all the enabled channels, not from a single channel.

C. Event selection

We determine the criteria for the event selection by evaluating the hit sequence, total energy, θ_G , and angular resolution measure (ARM) $= (\theta_K - \theta_G)$, and also considering the distribution of the first hit positions of the events as follows.

- (1) It is either a Si-Si sequence or Si-CdTe-side sequence.
- (2) Total energy E satisfies the following conditions.
 - (2-a) $79.0 \text{ keV} < E < 83.0 \text{ keV}$ for the Ba data.

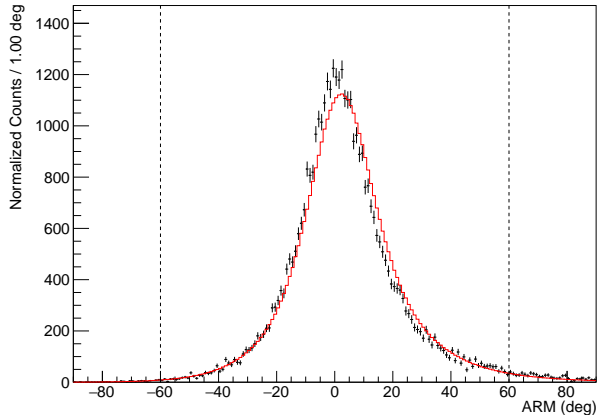


FIG. 5. ARM distributions of the events that satisfy all the selection criteria except for (4) (see text). Data points (black) show the Kr measurement minus the background. Solid line (red) shows the simulation. Dotted lines show criterion (4). Discrepancies between the data and the simulation could result from the energy-spectral distortion (low-energy tail) of the CdTe detectors which could not be simulated.

(2-b) $73.0 \text{ keV} < E < 77.5 \text{ keV}$ for the Kr data.

These threshold values correspond to the FWHM of the peak in question.

(3) Geometrical scattering angle θ_K satisfies $50.0^\circ < \theta_K < 170.0^\circ$. Fig. 4 shows this condition.

(4) $-60.0^\circ < \text{ARM} < 60.0^\circ$ (see Fig. 5).

(5) First hit position (x_1, y_1) satisfies $(x_1 - 14.25 \text{ mm})^2 + (y_1 - 4.0 \text{ mm})^2 < (40.25 \text{ mm})^2$. We find that the number of first-hit events is significantly smaller in some regions in distribution plots of first-hit positions (bottom-left pixels in Fig. 6). This could be caused by some assemblies in front of the EBIT-CC. We impose this condition to exclude such regions.

If an event does not satisfy all the conditions above, the event is excluded.

D. Monte Carlo simulation

We performed a series of Monte Carlo simulations to obtain the azimuthal distribution model $d_i^{(\text{model})}$ (see Sec. II for the context and notations). We utilized the `ComptonSoft` simulation toolkit¹⁶ for the simulations. `ComptonSoft` can simulate the physical processes in the detector including Compton scattering, the photoelectric effect, and the Doppler broadening^{17,27}. It employs the `Geant4` simulation framework^{1,2} for physical calculations.

Since the EBIT-CC is a multi-layer, pixelated detector, the detector response has some non-uniformity with

respect to the position of scattering \vec{x}_S . This non-uniformity could result from anisotropy of the radiation from sources, since we assume isotropic radiation in the simulation. To compensate for the non-uniformity, we split simulated events into 16 divisions with respect to the scattering position projected onto the xy plane (x_S, y_S) . Since they satisfy $-25.6 \text{ mm} < x_S < +25.6 \text{ mm}$ and $-25.6 \text{ mm} < y_S < +25.6 \text{ mm}$, we made 4 divisions with the area of $12.8 \text{ mm} \times 12.8 \text{ mm}$ along both the x and y directions and multiply a scaling factor ν_j ($j = 1, 2, \dots, 16$) for each division. The content of the i -th bin of the energy spectrum $e_{i'}$ is calculated as

$$e_{i'} = \sum_{j=1,2,\dots,16} \nu_j e_{i'j}, \quad (4)$$

where $e_{i'j}$ is the content of the i -th bin of j -th energy spectrum. The distribution of ϕ is calculated in the same manner. Specifically, ν_j are calculated by fitting the energy spectra.

To verify the simulation parameters, we simulated gamma-rays radiated from a ^{133}Ba point source and compared the simulation result with the measured one with the EBIT-CC. The measured and simulated energy spectra of the gamma-rays are shown in Fig. 7. We find the two spectra to agree well. Figs. 8 and 9 compare the azimuthal angular distributions and modulation curves, respectively, from the actual measurement and simulation. We find from the latter a small modulation proportional to $\cos(2\phi - \text{const.})$, which implies that the gamma-rays from the ^{133}Ba source are unpolarized. In Sec. V, we discuss systematic uncertainties on the degree of polarization using this curve.

V. RESULTS AND DISCUSSION

A. Results

The count rate of the all registered events was $\sim 2.3 \times 10^2 \text{ s}^{-1}$ both for the Ge detector and the EBIT-CC. Among 3.8×10^7 events recorded with the EBIT-CC, 4.3×10^4 events (0.11%) were selected.

1. Energy spectra (comparison with those of the Ge detector)

The energy spectra obtained with the Ge detector and Compton camera are shown in Fig. 10. For the latter, the events of the Si-Si and Si-CdTe-side sequences are used.

Using Fig. 10, we evaluate the calibration error. The radiative recombination lines of Kr ions is clearly present at around 75 keV in both spectra. This peak contains two components, namely radiative recombination lines into fully-ionized and hydrogen-like Kr. The difference in energy of the two is 0.640 keV¹¹. By fitting the peak of the spectrum from the Ge detector

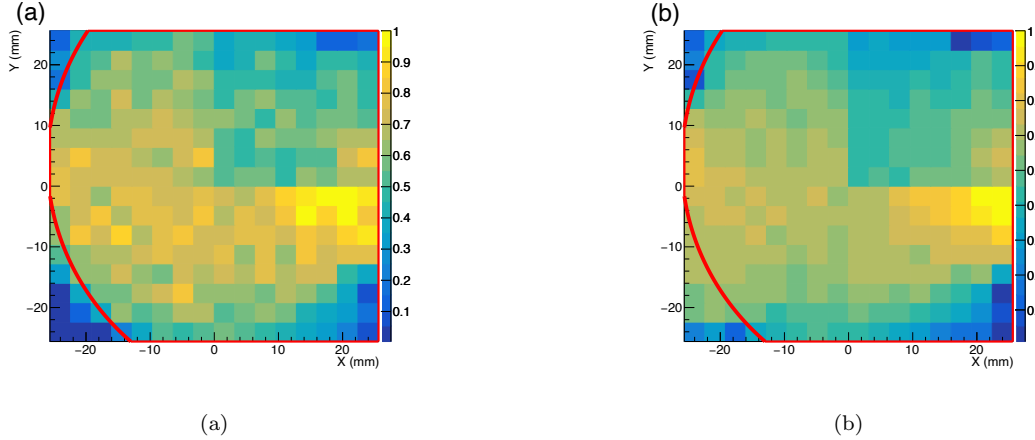


FIG. 6. Distributions of first-hit positions of the events that satisfy all the selection criteria except for (5) (see text). (a) and (b) show the Kr measurement minus the background and the simulation, respectively. Both distributions are normalized such that the maximum bin content is equal to 1. Some pixels at the bottom-left in (a) contain less events than those in (b). The top-right quarter parts in the both distributions contain less events than the other parts because we disabled a significant number of Si layers located there for their electric device troubles. Red lines show criterion (5).

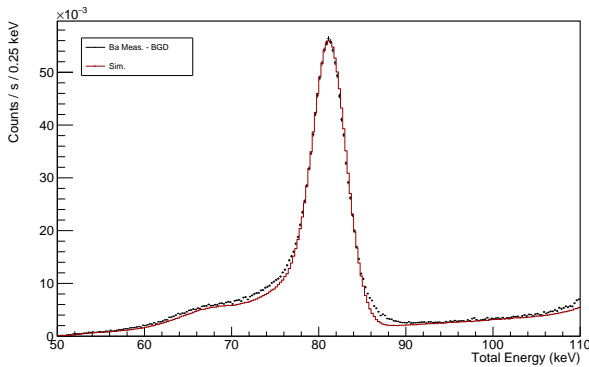


FIG. 7. Measured background-subtracted energy spectra (in black) of the gamma rays from a ^{133}Ba point source, overlaid with the simulation (red solid line). The used events are of the Si-Si and Si-CdTe-side sequences.

with two Gaussian functions whose peak energies differ by 0.640 keV, the peak energies are derived to be 75.35 ± 0.03 keV (hydrogen-like) and 75.99 ± 0.03 keV (fully-ionized), which as a whole correspond to the peak at 75.5 ± 0.2 keV for the Compton camera. The intensity-weighted average of the two peak positions in the Ge-detector spectrum is 75.68 ± 0.02 keV, which is consistent with the peak position in the Compton-camera spectrum.

The two-dimensional histograms of the energy deposit on the scatterer E_S versus energy deposit on the absorber E_A are plotted in Fig. 11. The lower bound at around $E_S \sim 7$ keV of each two-dimensional histogram results from the energy threshold of the Si detectors. The Kr-measurement histogram shows a stripe pattern that roughly follows $E_S + E_A \simeq 75$ keV, which should correspond to the spectral peak in Fig. 10.

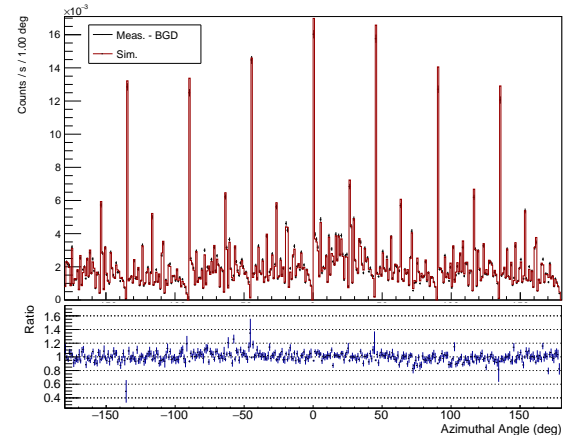


FIG. 8. Measured azimuthal angular distribution (in black) for the gamma rays from a ^{133}Ba point source, overlaid with the simulation (red solid line). The used events are of the Si-Si and Si-CdTe-side sequences and their energy range is 79.0 keV – 83.0 keV. The background is subtracted. Lower panel shows the ratio (in blue) of the measurement to simulation.

2. ϕ distributions and modulation curves

The degree of polarization, Π , of the detected x-rays is derived as follows. First, we construct ϕ histograms (designated as d_{ij}) and energy histograms ($e_{i'j}$) from the data of the Kr measurement, background measurement, and a pair of simulations on the basis of 100% polarized and unpolarized x-rays. Here, i' and i denote the bin number and j the index of division (see Section IV). The background data ($e_{i'j}^{(\text{bg})}$ and $d_{ij}^{(\text{bg})}$) are normalized

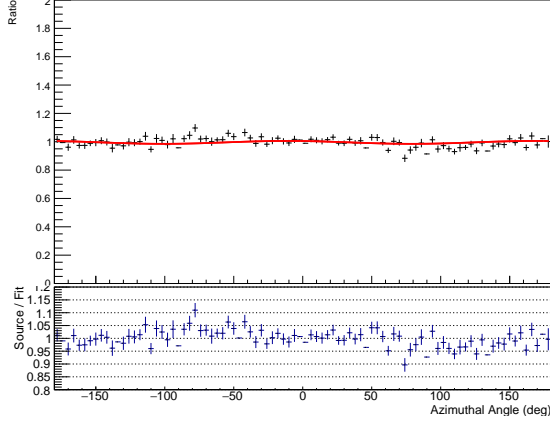


FIG. 9. Modulation curve for the gamma rays from a ^{133}Ba source, overlaid with the best-fit model function (red solid line), which is a linear superposition of a constant and $\cos(2\phi - \text{const.})$. The background is subtracted from the data. Lower panel shows the ratio (in blue) of the data to best-fit result.

such that the observation time is equal to that of the Kr data. To obtain the normalization factors ν_j for the simulation data, we fit the energy histograms of the Kr experiment ($e_{ij}^{(\text{exp})}$) with the model ($e_{ij}^{(\text{model})}$) for each of $i' = 1, 2, \dots, N'_{\text{bin}}$ and $j = 1, 2, \dots, 16$. The model is given by

$$e_{i'j}^{(\text{model})}(\Pi) = e_{i'j}^{(\text{bg})} + \nu_j \left((1 - \Pi)e_{i'j}^{(0)} + \Pi e_{i'j}^{(100)} \right), \quad (5)$$

where the superscripts (0) and (100) denote the simulation data for unpolarized and 100%-linearly-polarized x-rays, respectively. We compute the logarithmic likelihood ($M(\Pi)$) for the comparison between $d_{ij}^{(\text{exp})}$ and $d_{ij}^{(\text{model})}$ with fixed ν_j , as given by

$$M(\Pi) = \sum_{ij} \left(d_{ij}^{(\text{exp})} \ln d_{ij}^{(\text{model})} - d_{ij}^{(\text{model})} \right) + \text{const.} \quad (6)$$

where

$$d_{ij}^{(\text{model})}(\Pi) = d_{ij}^{(\text{bg})} + \nu_j \left((1 - \Pi)d_{ij}^{(0)} + \Pi d_{ij}^{(100)} \right) \quad (7)$$

for a range of $i = 1, 2, \dots, N_{\text{bin}}$. In Eq. (6), we assume that $d_{ij}^{(\text{exp})}$ obey Poisson distributions with the mean $d_{ij}^{(\text{model})}$. We iterate the procedure updating the Π value until $M(\Pi)$ reaches its maximum. Fig. 12 gives the block diagram that summarizes the procedure.

Fig. 13 shows the resultant summed histograms of ϕ with the best-fit result. We find that $M(\Pi)$ takes its maximum at $\Pi = 0.962$ (0.953-0.970; 1σ confidence). Fig. 14 shows the derived logarithmic likelihood curve.

Fig. 15 shows the obtained modulation curve. We find $\Pi = 0.968 \pm 0.010$ (1σ) by fitting the curve with the

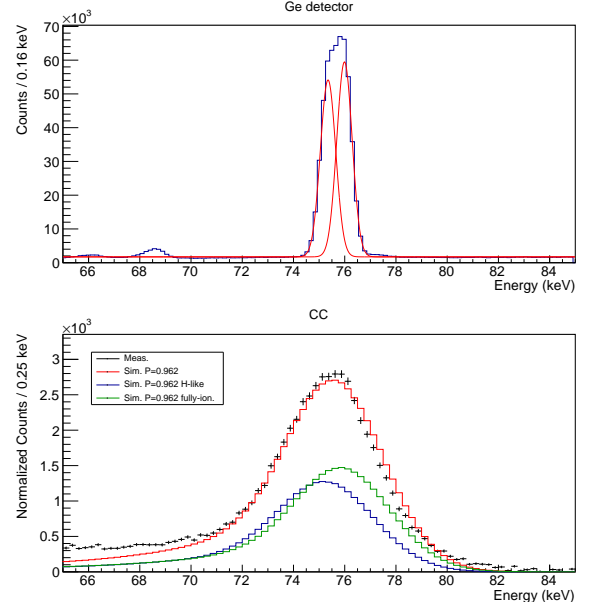


FIG. 10. Energy spectra of the Kr measurements. (Top panel) Spectrum with the Ge detector. Red lines show the derived peaks (see text). (Bottom panel) The spectrum with the EBIT-CC for the events of the Si-Si and Si-CdTe-side sequences. Black dots show the measured data minus the background. Red line shows the simulation for $\Pi = 0.962$ (the best fit). Blue and green lines show the simulated hydrogen-like and fully-ionized Kr lines, respectively.

function

$$\frac{d^{(\text{exp})}(\phi) - d^{(\text{bg})}(\phi)}{d^{(0)}(\phi)} = A(1 + Q \cos 2(\phi - \phi_0)), \quad (8)$$

where A , Q , and ϕ_0 are the fitting parameters; Q is the so-called modulation factor. Since the modulation factor is proportional to the degree of polarization, we obtain $\Pi = Q/Q_{100}$ where Q_{100} is the modulation factor for $d^{(100)}/d^{(0)}$.

B. Discussion

We evaluate the systematic uncertainty in the Monte Carlo simulation. In Fig. 9, we find the modulation factor $Q = 0.010$, which would correspond to $\Pi \sim 0.015$ under an assumption of $Q_{100} \sim 0.7$. Then, we interpret this value as the uncertainty of the simulation, $\Delta\Pi \sim 0.015$.

We conjecture that the systematic uncertainty resulting from the event selection is relatively small. We find that Π is fairly insensitive to the threshold of θ_K and ARM. Specifically, the optimal value of Π varies from 0.958 to 0.962 when we vary the threshold of θ_K for ranges of $0^\circ < \min \theta_K < 70^\circ$ and $130^\circ < \max \theta_K < 170^\circ$, and from 0.962 to 0.968 when we vary the threshold of ARM from $\pm 60^\circ$ to $\pm 10^\circ$. These variations are

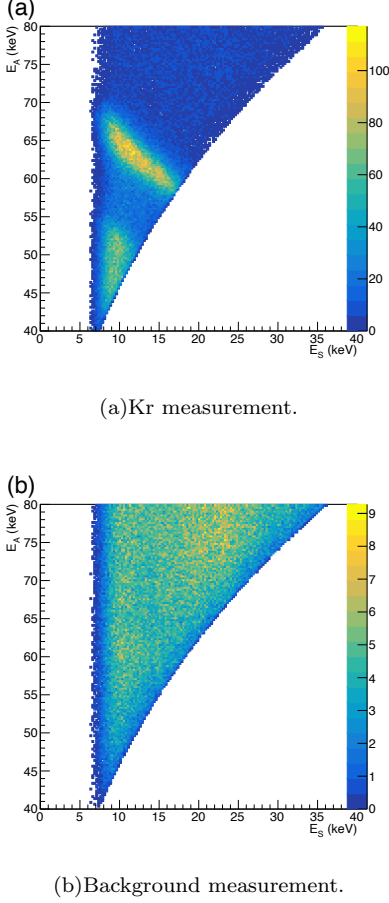


FIG. 11. Two-dimensional histograms of the energy deposit on the scatterer E_S versus energy deposit on the absorber E_A . (a) is for the Kr measurement and (b) for the background measurement. The histograms for the Kr and background measurements are normalized with respect to the Kr measurement.

smaller than the statistical uncertainty of Π . The uncertainty resulting from the detector non-uniformity (see Sec. IV) is within the statistical errors.

We find the systematic uncertainty resulting from the experimental setup to be sufficiently small. The spiral motion of the electron beam could not result in significant uncertainties, because the angle between the beam axis and the momentum of electrons is evaluated to be smaller than $\sim 4^\circ$. The misalignment between the directions of the x-rays and the azimuth of the Compton camera could not be larger than 1° . The size of the x-ray emitting region, approximately $60 \mu\text{m} \times 10 \text{ mm}$, would be small enough to be treated as a point source, in comparison with the angular resolution of the EBIT-CC.

Given the systematic uncertainties discussed above, we conclude $\Pi = 0.962 \pm 0.008$ (statistical) ± 0.015 (systematic), or $\Pi = 0.962 \pm 0.023$ if we combine the statistical and the systematic uncertainties. In other words, we have obtained the degree of polarization with

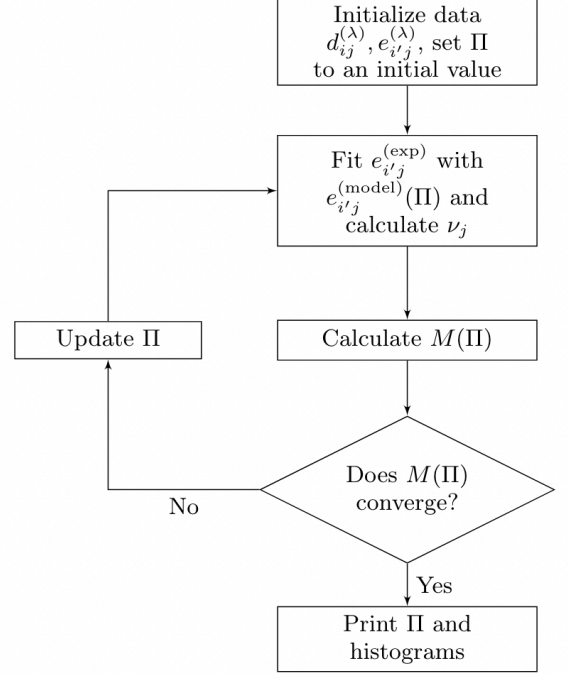


FIG. 12. Schematic diagram of the procedure to find the optimal degree of polarization Π . Note $\lambda = \text{exp, bg, 0, or 100}$. Definitions of d_{ij} , $e_{i'j}$, ν_j , and $M(\Pi)$ are presented in the text.

an error of $\sim 2\%$.

The method that we have presented in this paper is applicable also to other line emissions, such as the dielectronic recombination x-rays of heavy ions. For example, it is theoretically expected that the polarization degree of dielectronic recombination x-rays depends on the zero-frequency approximation in the Breit interaction^{4,14,23}. To determine the limit of the approximation, one would need an absolute precision of $\Delta\Pi \sim 0.02$ for highly charged bismuth (Bi) ions, for the expected $\Pi \sim 0.2$. It would be reasonable to conclude that these criteria can be achieved by applying our method.

VI. SUMMARY AND CONCLUSION

We developed the EBIT-CC, a novel Compton polarimeter with Si/CdTe semiconductor detectors, and attached it on the Tokyo-EBIT in the UEC. An experiment was performed to evaluate its polarimetric capability through an observation of radiative recombination x-rays emitted from highly charged Kr ions that was generated by the Tokyo-EBIT. The Compton camera was calibrated for the $\sim 75 \text{ keV}$ x-rays. We developed event reconstruction and selection procedures and applied them to every registered event. As a result, we obtained the degree of polarization $\Pi = 0.962 \pm 0.023$. This preci-

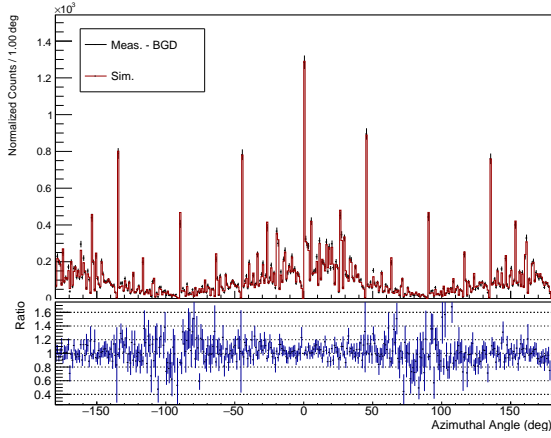


FIG. 13. Azimuthal angular distribution of the Kr measurement (in black), overlaid with the simulation result for $\Pi = 0.962$ (the best-fit result) in the red histogram. The events of the Si-Si and Si-CdTe-side sequences are selected. Lower panel shows the ratio (in blue) of the measured data to simulation.

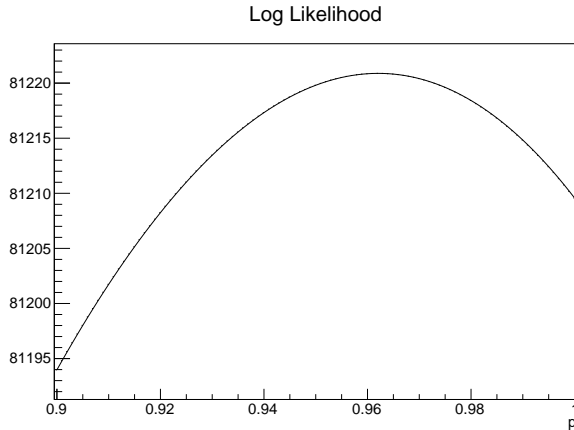


FIG. 14. Logarithmic likelihood $M(\Pi)$. The maximum value is found at $\Pi = 0.962$.

sion would be satisfactory for evaluation of the QED and relativistic effect, for which $\Delta\Pi \sim 0.02$ for $\Pi \sim 0.2$ is required. To conclude, we have established a new polarimetric method using the EBIT-CC, which shows sufficient polarimetric capability and sensitivity for high- Z atomic x-ray observations.

ACKNOWLEDGEMENTS

This work was supported by JSPS KAKENHI Grant-in-Aid for Scientific Research on Innovative Areas ‘Toward new frontiers: Encounter and synergy of state-of-the-art astronomical detectors and exotic quantum beams’ 18H05458, 18H05463 and 19H05187, Grant-in-Aid for Scientific Research (A) 20H00153, World Premier

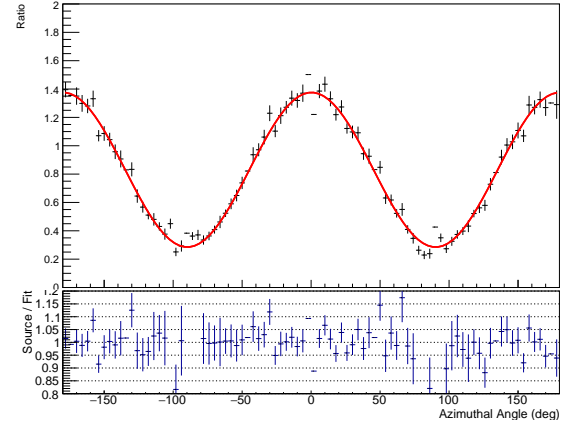


FIG. 15. Modulation curve for the Kr radiative recombination, where the background is subtracted. Red line shows the best-fit model function, which consists of a constant and $\cos(2\phi - \text{const.})$. Lower panel shows the ratio (in blue) of the data to best-fit result.

International Research Center Initiative (WPI), MEXT, Japan, and JST-SENTAN program (Development of an advanced gamma-ray imaging system with an ultra-wide field of view and a high sensitivity).

DATA AVAILABILITY

The data that support the findings of this study are available from the corresponding author upon reasonable request.

- ¹S. Agostinelli et al. Geant4—a simulation toolkit. *Nuclear Instruments and Methods in Physics Research Section A: Accelerators, Spectrometers, Detectors and Associated Equipment*, 506(3):250–303, 2003.
- ²J. Allison et al. Geant4 developments and applications. *IEEE Transactions on Nuclear Science*, 53(1):270–278, Feb 2006.
- ³P. Beiersdorfer et al. Measurement and interpretation of the polarization of the x-ray line emission of heliumlike Fe XXV excited by an electron beam. *Phys. Rev. A*, 53:3974–3981, Jun 1996.
- ⁴S. Fritzsche, A. Surzhykov, and T. Stöhlker. Dominance of the Breit interaction in the x-ray emission of highly charged ions following dielectronic recombination. *Phys. Rev. Lett.*, 103:113001, Sep 2009.
- ⁵E. Haug. On the nonthermal excitation and polarization of x-ray lines during solar flares. *Solar Physics*, 61:129–142, 1979.
- ⁶G. Herrmann. Optical theory of thermal velocity effects in cylindrical electron beams. *Journal of Applied Physics*, 29(2):127–136, 1958.
- ⁷Hitomi Collaboration. Detection of polarized gamma-ray emission from the Crab nebula with the Hitomi Soft Gamma-ray Detector. *Publications of the Astronomical Society of Japan*, 70(6), 11 2018. 113.
- ⁸J. Katsuta et al. Study of the polarimetric performance of a Si/CdTe semiconductor Compton camera for the Hitomi satellite. *Nuclear Instruments and Methods in Physics Research Section A: Accelerators, Spectrometers, Detectors and Associated Equipment*, 840:51–58, 2016.

- ⁹O. Klein and Y. Nishina. Über die Streuung von Strahlung durch freie Elektronen nach der neuen relativistischen Quantendynamik von Dirac. *Zeitschrift für Physik*, 52:853–868, 1929.
- ¹⁰J. B. Mann and W. R. Johnson. Breit interaction in multielectron atoms. *Phys. Rev. A*, 4:41–51, Jul 1971.
- ¹¹Nobuyuki N. et al. The 1s Lamb shift in hydrogenlike rhodium measured with an electron beam ion trap. *Journal of the Physical Society of Japan*, 72(7):1650–1654, 2003.
- ¹²N. Nakamura. Breit interaction effect on dielectronic recombination of heavy ions. *Journal of Physics B: Atomic, Molecular and Optical Physics*, 49(21):212001, oct 2016.
- ¹³N. Nakamura et al. An overview of the Tokyo electron beam ion trap. *Physica Scripta*, T73:362–364, jan 1997.
- ¹⁴N. Nakamura et al. Evidence for strong Breit interaction in dielectronic recombination of highly charged heavy ions. *Phys. Rev. Lett.*, 100:073203, Feb 2008.
- ¹⁵Here we simplify the processes of photons. In fact, other sequences of processes are possible. For example, a photon can be scattered by the scatterer and also absorbed by the scatterer.
- ¹⁶H. Odaka et al. Development of an integrated response generator for Si/CdTe semiconductor Compton cameras. *Nuclear Instruments and Methods in Physics Research Section A: Accelerators, Spectrometers, Detectors and Associated Equipment*, 624(2):303–309, 2010. New Developments in Radiation Detectors.
- ¹⁷C. E. Ordonez et al. Doppler broadening of energy spectra in Compton cameras. In *1997 IEEE Nuclear Science Symposium Conference Record*, volume 2, pages 1361–1365 vol.2, Nov 1997.
- ¹⁸C. Shah et al. Polarization measurement of dielectronic recombination transitions in highly charged krypton ions. *Phys. Rev. A*, 92:042702, Oct 2015.
- ¹⁹E. H. Silver et al. Bragg crystal polarimeters. *Optical Engineering*, 29(7):759 – 766, 1990.
- ²⁰H. Tajima et al. Design and performance of Soft Gamma-ray Detector onboard the Hitomi (ASTRO-H) satellite. *Journal of Astronomical Telescopes, Instruments, and Systems*, 4(2):1 – 14, 2018.
- ²¹T. Takahashi et al. Hard x-ray and γ -ray detectors for the NeXT mission. *New Astronomy Reviews*, 48(1):269–273, 2004. Astronomy with Radioactivities IV and Filling the Sensitivity Gap in MeV Astronomy.
- ²²S. Takeda et al. Demonstration of in-vivo multi-probe tracker based on a Si/CdTe semiconductor Compton camera. *IEEE Transactions on Nuclear Science*, 59(1):70–76, Feb 2012.
- ²³X. M. Tong et al. Mechanism of dominance of the Breit interaction in dielectronic recombination. *Journal of Physics B: Atomic, Molecular and Optical Physics*, 48(14):144002, may 2015.
- ²⁴H. Watanabe et al. Characteristics of the Tokyo electron-beam ion trap. *Journal of the Physical Society of Japan*, 66(12):3795–3800, 1997.
- ²⁵S. Watanabe et al. A Si/CdTe semiconductor Compton camera. *IEEE Transactions on Nuclear Science*, 52(5):2045–2051, Oct 2005.
- ²⁶S. Watanabe et al. The Si/CdTe semiconductor Compton camera of the ASTRO-H Soft Gamma-ray Detector (SGD). *Nuclear Instruments and Methods in Physics Research Section A: Accelerators, Spectrometers, Detectors and Associated Equipment*, 765:192 – 201, 2014. HSTD-9 2013 - Proceedings of the 9th International 'Hiroshima' Symposium on Development and Application of Semiconductor Tracking Detectors.
- ²⁷A. Zoglauer and G. Kanbach. Doppler broadening as a lower limit to the angular resolution of next-generation compton telescopes. In J. E. Truemper and H. D. Tananbaum, editors, *X-Ray and Gamma-Ray Telescopes and Instruments for Astronomy*, volume 4851, pages 1302 – 1309. International Society for Optics and Photonics, SPIE, 2003.